ACS APPLIED NANO MATERIALS

www.acsanm.org Article

# Flexible Memristor Devices Using Hybrid Polymer/Electrodeposited GeSbTe Nanoscale Thin Films

Ayoub H. Jaafar,* Lingcong Meng, Tongjun Zhang, Dongkai Guo, Daniel Newbrook, Wenjian Zhang, Gillian Reid, C. H. de Groot, Philip N. Bartlett,* and Ruomeng Huang*

Cite This: *ACS Appl. Nano Mater.* 2022, 5, 17711−17720 Read Online

ACCESS | Metrics & More | Article Recommendations | Supporting Information

**ABSTRACT:** We report on the development of hybrid organic−inorganic material-based flexible memristor devices made by a fast and simple electrochemical fabrication method. The devices consist of a bilayer of poly(methyl methacrylate) (PMMA) and Te-rich GeSbTe chalcogenide nanoscale thin films sandwiched between Ag top and TiN bottom electrodes on both Si and flexible polyimide substrates. These hybrid memristors require no electroforming process and exhibit reliable and reproducible bipolar resistive switching at low switching voltages under both flat and bending conditions. Multistate switching behavior can also be achieved by controlling the compliance current (CC). We attribute the switching between the high resistance state (HRS) and low resistance state (LRS) in the devices to the formation and rupture of conductive Ag filaments within the hybrid PMMA/GeSbTe matrix. This work provides a promising route to fabricate flexible memory devices through an electrodeposition process for application in flexible electronics.

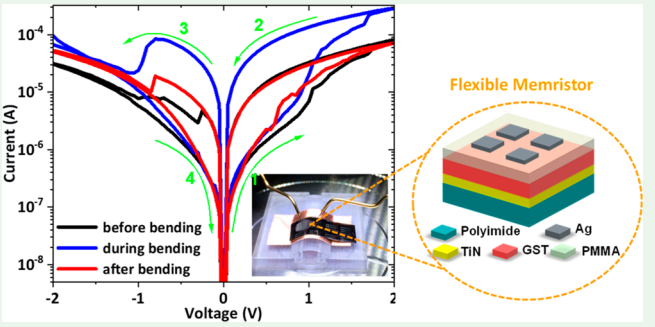


**KEYWORDS:** *Flexible, electrodeposition, hybrid material, resistive switching, multilevel states*

## 1. INTRODUCTION

Fabrication of modern electronic devices on a bendable substrate is essential for the future development of foldable, stretchable, and wearable electronic applications.[1] This new class of electronics enables new product paradigms that are not possible with conventional semiconductors and rigid substrates, while offering the advantages of low cost and light weight.[2] The past decades have witnessed remarkable progress for flexible electronics in many sectors including consumer electronics, automotive, retail, and healthcare.[3,4] As a fundamental component of all modern electronic system, research on flexible electronic memory has attracted tremendous attention with several categories of memory devices proposed.[5] Resistive switching based memristor devices can store and process information and are considered among the most promising candidates for next generation memory due to their simple structure, low power consumption, excellent storage capability, and scalability.[6−13]

Typically, a resistive memristor consists of a simple metal−insulator−metal (MIM) structure where the resistive switching material is sandwiched between two electrodes. The switching between the low resistance state (LRS) and high resistance state (HRS) is achieved by the creation and disruption of conductive filaments which are made of either metallic atoms from the active electrode or the defects within the switching layer.[14] Memristors based on flexible substrates have been extensively researched over the past decade, while various materials have been investigated as the switching layer, such as organic materials,[15,16] 2D materials,[17,18] metal oxides,[19−21] graphene oxide,[22] and perovskites.[23] Semiconductor chalcogenide based memristors have demonstrated increasing potential due to their excellent scalability and compatibility with CMOS circuits.[24] The most widely used semiconductor chalcogenide GeSbTe has seen extensive usage in phase-change memory (PCM).[25] The data storage in PCM relies on the rapid and reversible switch between the amorphous (high resistance) and crystalline (low resistance) phase of the material. This involves a melt-quenching reset process that requires a high programming current, which has become the major obstacle for the integration of PCMs.[26] Resistive switching, however, does not involve major structural phase changes, and the switching between the HRS and LRS and vice versa can be achieved at lower voltages upon change the polarity of the applied electric field.[27] Resistive switching effects have been observed in several chalcogenides such as AgGeSe, AgGeTe,

Received: August 17, 2022
Accepted: November 2, 2022
Published: November 25, 2022

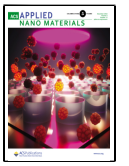

AgInSbTe, and GeSbTe, with switching mechanisms attributed to a formation and rapture of conductive filaments either from the migration of metal cations (e.g., Ag and Cu)[28−36] in the electrochemical metallization (ECM) process or from migration of Sb and Te ions inside the chalcogenide materials.[27,37−41]

Conventionally, chalcogenide materials are deposited via techniques such as physical vapor deposition, chemical vapor deposition, and atomic layer deposition.[42] These "top-down" approaches often require vacuum equipment, which leads to high deposition costs and slow deposition rates. Additionally, their high thermal budgets can also be prohibitive for their application in flexible application. Electrodeposition is a well-established deposition method in the electronic industry that offers a low-cost and fast alternative solution for chalcogenide deposition.[43,44] Our group has previously reported the electrodeposition of amorphous ternary GeSbTe thin films from a single, highly tunable, nonaqueous electrolyte,[45,46] demonstrating both phase-change and resistive switching properties in highly scalable cross-bar architectures.[41,47] More importantly, electrodeposition is a low-temperature deposition technique which makes it highly suitable for deposition onto flexible substrates. However, the deposition of a nanoscale thin film chalcogenide-based memristor onto flexible substrate via electrodeposition has never been reported.

In addition, hybrid organic−inorganic material-based memristors have attracted attention since they combine the electronic properties of inorganic components and the solution processing advantages of organic components.[48−53] In comparison to inorganic material-based memristors, hybrid memristors have demonstrated improved switching properties such as high ON/OFF ratio, ultralow operating voltage, reduced power consumption, as well as having various advantages such as multilevel data storage, analogue switching, and flexibility.[54−59]

In this work, we report the development of high-quality hybrid memristor devices that are fabricated by electrodeposition. The hybrid memristor devices consist of a bilayer of electrodeposited GeSbTe nanoscale thin films combined with different thicknesses of an insulating PMMA layer (the thickness is controlled by changing the PMMA concentration) sandwiched between a TiN bottom electrode and an Ag top electrode using Si and polyimide substrates. The hybrid devices demonstrate desirable memristor properties such as a free forming process, low operation voltages, good cycling endurance, multistate switching behavior, and, importantly, mechanical flexibility. These properties open the route to realize fully the potential of memristor devices for low-cost and high-performance flexible electronics.

## 2. RESULTS AND DISCUSSION

Figure 1 shows a schematic of the electrodeposition setup using a potentiostat connected to a TiN electrode through a Cr/Au global contact. The depositions were performed in a three-electrode cell including a Pt/Ir (90:10%) disc as a counter electrode and a Ag/AgCl wire in a glass frit containing 0.1 M $[N^nBu_4]Cl$ in dichloromethane ($CH_2Cl_2$) as a reference electrode. Electrodeposition of GeSbTe thin film was carried out in a dichloromethane (DCM) solution using precursors for Ge, Sb, and Te synthesized in-house.[60] Prepatterned TiN thin films on $Si/SiO_2$ substrates were used as the deposition electrode. The details of TiN electrode fabrication were reported in our previous work.[46] Prior to the film deposition,

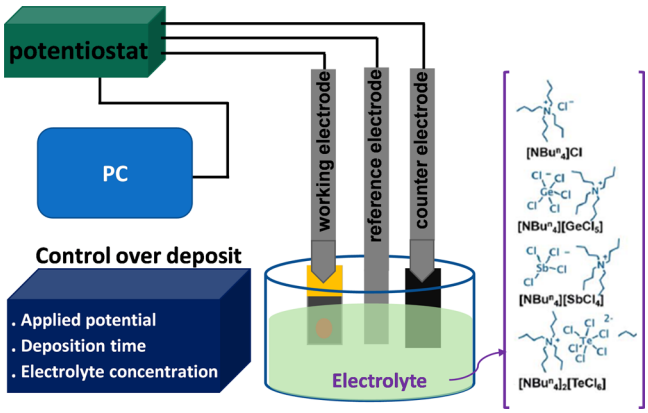


**Figure 1.** Schematic of the electrodeposition setup containing the chip connected through its global electrode to the potentiostat, together with the molecular structure of the precursors used in the dichloromethane solvent.

cyclic voltammetry (CV) was recorded as shown in Figure 2a. The four shoulders at approximately −0.1 V, −0.9 V, −1.3 V, and −1.75 V correspond with the reduction of $Ge^{4+}$ to $Ge^{2+}$,

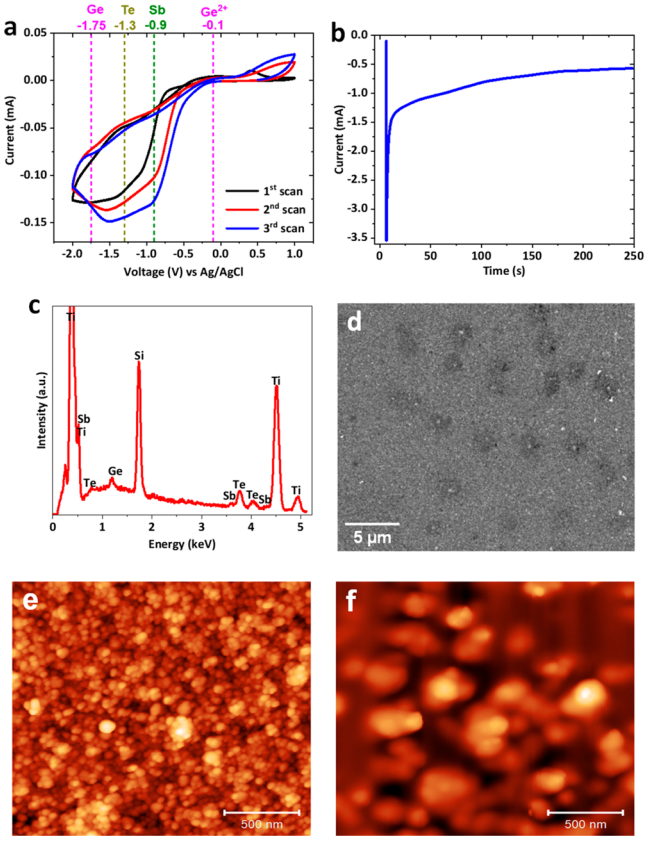


**Figure 2.** (a) Cyclic voltammogram of the 4-mm-diameter TiN/$SiO_2$/Si substrate in 0.1 M $[N^nBu_4]Cl$ electrolyte containing 2.5 mM $[N^nBu_4]GeCl_5$, 1 mM $[N^nBu_4]SbCl_4$, and 2 mM $[N^nBu_4]_2TeCl_6$. Scan rate: 50 mV $s^{-1}$. (b) Current time transient for GeSbTe electrodeposition at a deposition potential of −1.75 V vs Ag/AgCl. The cutoff charge is −5 μC. (c) EDX spectrum of the electrodeposited GeSbTe on a Si substrate showing the presence of Ge, Sb, and Te within the thin film. (d) Top SEM image for GeSbTe thin film. (e) AFM image of GeSbTe thin film. (f) AFM image of PMMA(50%)/GeSbTe bilayer.


https://doi.org/10.1021/acsanm.2c03639
ACS Appl. Nano Mater. 2022, 5, 17711−17720

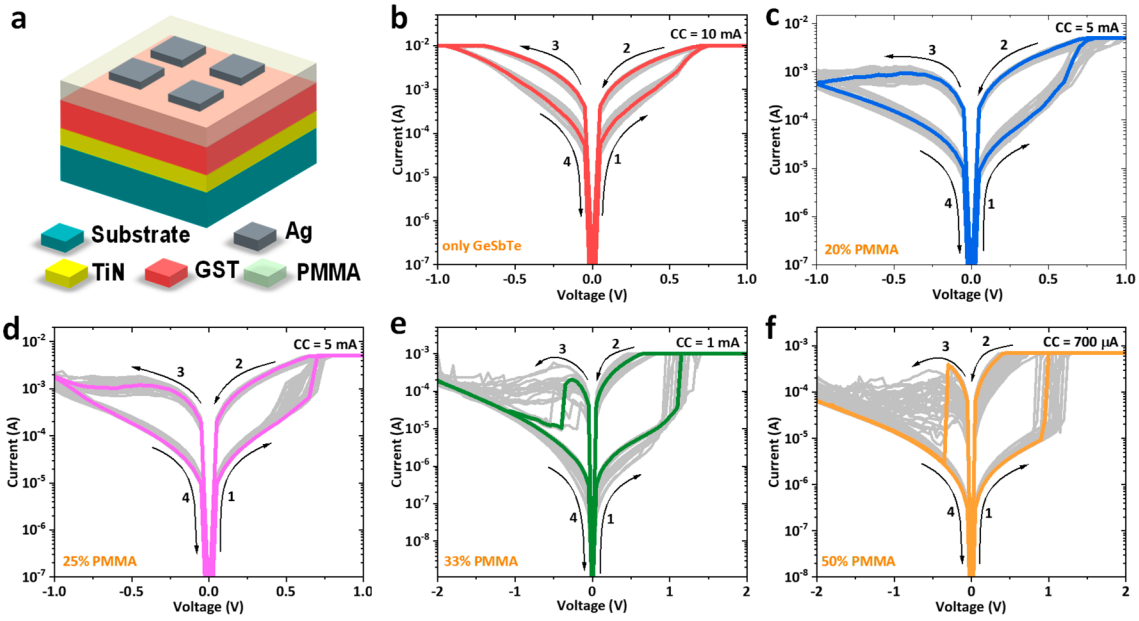


**Figure 3.** (a) Schematic of hybrid memristor devices. (b) *I*–*V* characteristics of a memristor consisting of a GeSbTe thin film (without PMMA) sandwiched between TiN and Ag electrodes, Ag/GeSbTe/TiN. (c–f) *I*–*V* characteristics of memristor consisting of hybrid PMMA/GeSbTe bilayer, Ag/PMMA/GeSbTe/TiN, with different concentrations of PMMA. The PMMA concentrations are 20% (c), 25% (d), 33% (e), and 50% (f).

$Sb^{3+}$, $Te^{4+}$, and $Ge^{2+}$ to Ge(0), respectively.[47,61] To ensure the incorporation of all three elements, the deposition potential of −1.75 V vs Ag/AgCl was selected. The detailed process of the electrodeposition is provided in the Experimental Section. The current–time transient of the deposition is shown in Figure 2b. Initial current spike is caused by double layer charging, followed by the current magnitude decreasing and reaching a steady state, indicating a diffusion controlled process. The film thickness was controlled by a cutoff charge of 5 $\mu$C to reach a nominal thickness of 100 nm.

The composition of the electrodeposited GeSbTe film was characterized by energy dispersive X-ray analysis (EDX) and the spectrum is presented in Figure 2c. The plot clearly shows the presence of all three elements in the GeSbTe thin film, without any significant impurities. The film is Te-rich, with a Ge:Sb:Te composition ratio of 12:10:78. Top view scanning electron microscopy (SEM) and atomic force microscopy AFM images of the electrodeposited GeSbTe thin film are shown in Figure 2d and e, respectively. The images show that the film is uniformly deposited on the substrate and consists of granules with sizes of ca. 50 nm. Poly(methyl methacrylate) (PMMA) films were subsequently coated on the GeSbTe films to form a PMMA/GeSbTe hybrid material (details in the Experimental Section). An AFM image of the hybrid material with 50% concentration of PMMA is shown in Figure 2f. Note that the roughness of the GeSbTe thin film, Figure 2e, is 9.38 nm, whereas the roughness of the PMMA/GeSbTe bilayer, Figure 2f, is 14.84 nm. The thickness of the PMMA film is controlled by the concentration of the PMMA solution (PMMA to anisole ratio), where a higher concentration will lead to a thicker film. The thickness of PMMA as a function of solution concentration is shown in the Supporting Information Figure S1. The memristor fabrication process is completed by patterning Ag top electrodes on the hybrid organic–inorganic structure using thermal evaporation technique.

Figure 3a schematically describes the developed hybrid organic–inorganic memristor based on the PMMA/GeSbTe bilayer structure. We first investigate the electronic switching properties of a single layer GeSbTe-based memristor without PMMA. The DC-IV characteristic of the device is shown in Figure 3b with the direction of the current sweep indicated by arrows. The device is initially in a high resistance state (HRS) and could be switched to a low resistance state (LRS) using a positive DC sweep from 0 to 1 V under a compliance current (CC) of 10 mA. The RESET from the LRS to HRS was achieved by a negative DC sweep from 0 to −1 V, representing a typical bipolar switching behavior. It is worth noting that a CC was needed at the RESET process to limit the operating current and to protect the device from breakdown.[41,62,63] The absence of the CC during the RESET process switches the single-layer GeSbTe-based device to a higher operating current, resulting in breakdown of the device.[41] Subsequent DC-IV cycles (gray lines) are similar to the initial switching cycle (red line). This indicates that no electroforming process is required to initialize the devices for the resistive switching effect. Note that the electroforming process is needed to initiate the switching in oxides.[64] However, we expect the lack of the forming process in our devices due to a large amount of Te atoms within the Te-rich GeSbTe matrix, which can play a role in the formation of Te conductive filament(s). Both SET and RESET processes are characterized by gradual current change, and the device only operates at high current. Such high operating current is likely due to the formation of strong filament(s) within the GeSbTe layer. This is not surprising, as the granule-like texture of the as-deposited GeSbTe layer implies a certain amount of porosity in the film.[32,41] It has been suggested that the voids or pores in the electrolyte layer could serve to facilitate ion migration in the thin film for the electrochemical metallization (ECM) memories.[65] The voids or pores within the GeSbTe electrolyte can likely act as diffusion pathways for Ag cations, enabling the formation of


https://doi.org/10.1021/acsanm.2c03639
ACS Appl. Nano Mater. 2022, 5, 17711–17720

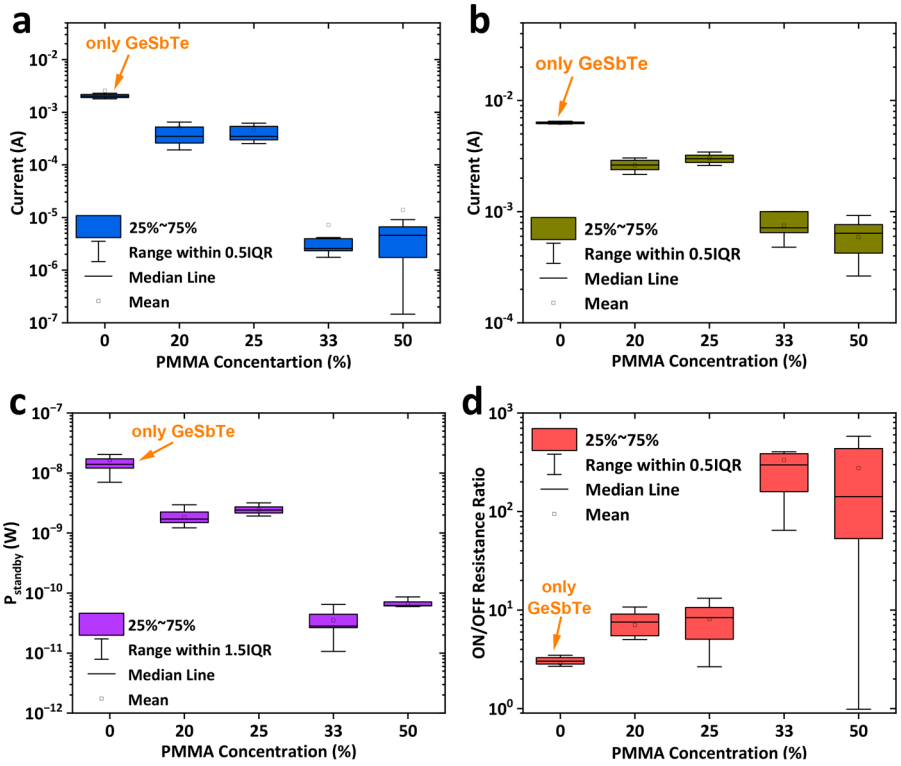


**Figure 4.** Resistive switching characteristics of hybrid Ag/PMMA/GeSbTe/TiN memristor devices on Si substrate. (a) OFF current versus PMMA concentration; (b) ON current versus PMMA concentration; (c) power consumption versus PMMA concentration; (d) ON/OFF ratio versus PMMA concentration. The OFF and ON currents and the ON/OFF resistance ratio were taken at a read voltage of 0.1 V.

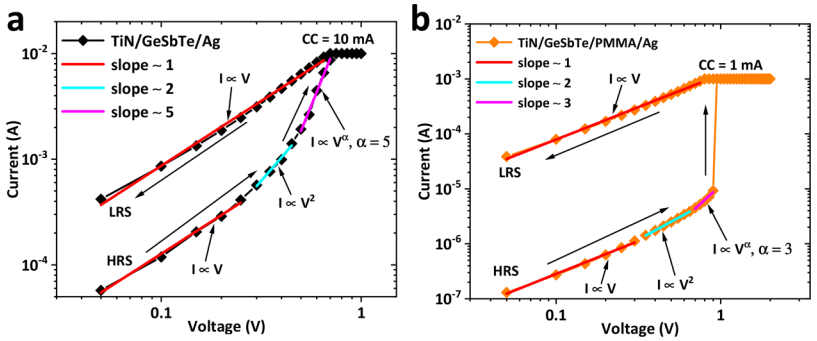


**Figure 5.** Current−voltage curves demonstrating fits to the SCLC mechanism for the HRS to LRS transition for a Ag/GeSbTe/TiN memristor device (a) and a hybrid Ag/PMMA/GeSbTe/TiN memristor device (50% PMMA) (b), both fabricated on Si substrates.

conductive nano Ag filament(s) across the device.[32] This high operating current leads to high power consumption which is highly undesirable for memristors.

The hybrid PMMA/GeSbTe-based memristor exhibits similar forming-free, bipolar resistive switching behavior to the single layer device (shown in Figure 3c−f). However, significant differences in the resistive switching properties can be observed. The most noticeable change is the lower CC required for the SET process. As the PMMA concentration in the solution increases from 20% to 50%, the CC required dropped by almost 1 order of magnitude from 5 mA to 700 $\mu$A with an associated reduction in power consumption. In addition, the voltage switching between the two resistance states changes from smooth to sharp for higher concentration of the PMMA layer. Another interesting feature is that all hybrid PMMA/GeSbTe-based devices do not require CC during the RESET process, facilitating subsequent circuit design. The DC endurance properties of the single layer and hybrid PMMA/GeSbTe devices are presented in Figure S2a−e. Retention testing for the hybrid TiN/PMMA/GeSbTe/Ag memristor (50% PMMA concentration) in both the HRS and LRS were examined at a continuous read voltage of 0.1 V for over 4000 s and are presented in Figure S2f.

To better understand the impact of the additional PMMA layer on the memristor switching properties, we plot the operating currents (at 0.1 V), the power consumption, and the ON/OFF resistance ratio of each device as a function of the PMMA concentration. Figure 4a,b shows the distribution of OFF and ON currents, respectively. The plots clearly show that increasing the PMMA concentration from 20% to 50% decreases both the OFF and ON currents. The plots also show the GeSbTe devices without the PMMA to have the highest OFF and ON currents, making our hybrid devices a promising candidate for low power consumption memories. Figure 4c


https://doi.org/10.1021/acsanm.2c03639
ACS Appl. Nano Mater. 2022, 5, 17711−17720

shows that the power consumption reduces from 570 nW for the GeSbTe thin film to only 11 nW for the hybrid PMMA/GeSbTe device (50% PMMA). The power consumption, ($P_{Standby} = I_{HRS} \times V_{read}$), was calculated at a read voltage of (100 mV) and the OFF currents of the devices. This notable control of the currents results in a significant improvement in the separation between the OFF and ON states and therefore enhances the ON/OFF resistance ratio from 8 to 836, as shown in Figure 4d. All these comparisons clearly suggest that the switching performance of the inorganic GeSbTe memristor can be significantly improved by the incorporating of an organic layer.

To explore the conduction mechanism in our control Ag/GeSbTe/TiN memristor and hybrid Ag/PMMA/GeSbTe/TiN memristor, the current−voltage curves were replotted in double-logarithmic scale as shown in Figure 5. The fitting results indicate a similar conduction mechanism for both devices. While the Ohmic conduction mechanism is dominant in the LRS state, the HRS state combines Ohmic conduction in the low applied voltage region, indicating conduction induced by thermally generated carriers, and space charge limited current (SCLC) in the high applied voltage region. A similar conduction mechanism is observed for the hybrid material-based devices with different concentrations of PMMA and is reported in Figure S3.

A switching mechanism consistent with the electrical data is proposed and displayed in Figure 6. The switching mechanism

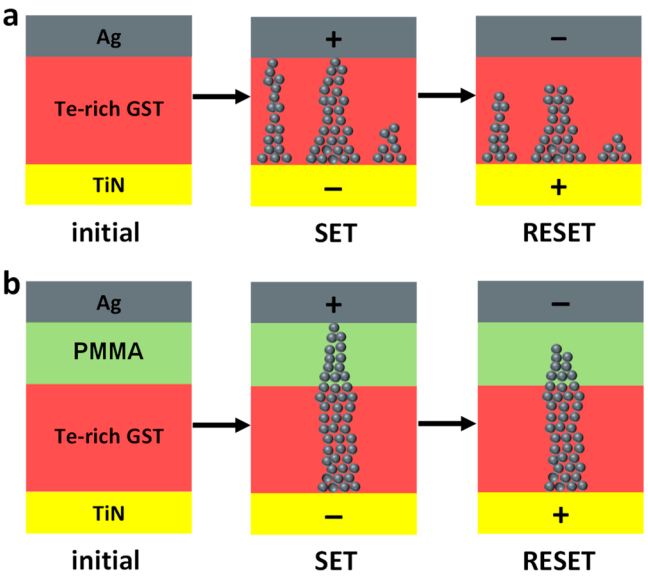


**Figure 6.** Schematic showing the proposed switching mechanism for (a) the single GeSbTe memristor and (b) the hybrid PMMA/GeSbTe memristor.

is based on the formation and rapture of conductive Ag filament(s) across the GeSbTe and the hybrid PMMA/GeSbTe layer upon application of different electric field polarities. In the case of a single-layer GeSbTe-based memristor, the switching mechanism occurs within the GeSbTe thin film, which serves as an electrolyte for the ECM process (Figure 6a).

In the case of the hybrid memristor, both PMMA/GeSbTe matrix can act as electrolyte, where a resistive switching through oxidation/reduction reactions (ECM process) can occur upon altering the polarity of the electric field (Figure 6b). The hybrid device is initially in the HRS (initial). Applying a positive potential to the top Ag electrode ionizes the Ag atoms ($Ag^+$) at the top Ag/PMMA interface. Under high electric field, the $Ag^+$ ions can move across the PMMA and GeSbTe to the bottom electrode, where the neutral Ag atoms are accumulated and start to form a filament. Once the grown filament connects to the top Ag electrode, the device switches to the LRS (SET). In contrast, applying a negative potential moves the $Ag^+$ ions formed at the bottom electrode to the top electrode and ruptures the preformed filament, switching the device back to the HRS (RESET).

The results obtained suggest that the PMMA layer plays a key role in improving the resistive switching properties. As a barrier between the GeSbTe and top electrode, the PMMA diminishes the penetration of the Ag atoms into the voids of the GeSbTe thin film. The PMMA also changes the switching between the two resistance states from a smooth transition for the GeSbTe device to a sharp transition for the hybrid PMMA/GeSbTe devices. For the devices containing only GeSbTe, multiple, large Ag filaments can easily be formed across the high porosity GeSbTe thin film upon application of high electric field. The large Ag filament(s) results in the high operating currents and is also responsible for the CC requirement during the RESET process. For the devices containing hybrid PMMA/GeSbTe material, the formation of Ag filaments across the hybrid material tends to be more restricted at high PMMA concentration, resulting in a sharp switching with 2 orders of magnitude difference between the LRS and HRS state. In addition, the PMMA makes the switching from the HRS to the LRS slower, as the SET voltage increases from ∼0.6 V for the devices containing only GeSbTe thin films to ∼1.7 V for the devices containing hybrid PMMA (50%)/GeSbTe material. The PMMA may also smooth the GeSbTe interface region and mask local surface defects and surface roughness[66] that can result in undesirable device properties such as switching the device to a higher current level and breakdown in the absence of CC during RESET process.[41] Protecting the GeSbTe with PMMA not only improves the resistive switching properties but also reduces the standby power consumption, which potentially suppresses the sneak current and devices disturbance issues.[18]

Multistate switching can be achieved in our hybrid PMMA/GeSbTe devices by controlling the CC level. Figure 7a demonstrates the current−voltage curves of a hybrid Ag/PMMA/GeSbTe/TiN memristor switched at different CC level with a sweep voltage of ±2 V. The plot shows that the device switches to different LRS values upon varying the CC level from 700 μA (red curve) to 1 mA (blue curve), while the HRS remained almost the same. Therefore, the device exhibits three distinct resistance states including one HRS and two LRS. The multistate switching behavior is uniform and reproducible for 50 cycles, as demonstrated in Figure 7b. Such behavior suggests that our hybrid memristor devices have promising potential as candidates of artificial synapses for neuromorphic computing and multilevel data storage applications.[67−70] Such CC level-dependent control has been widely demonstrated in resistive switching memories and can be ascribed by the formation of filaments with different dimensions across the device.[56,71] Although similar multistate switching behavior was previously observed in our crossbar GeSbTe-based memory devices, the ON/OFF resistance ratio was smaller (by about 1 order of magnitude), and the CC was


https://doi.org/10.1021/acsanm.2c03639
ACS Appl. Nano Mater. 2022, 5, 17711−17720

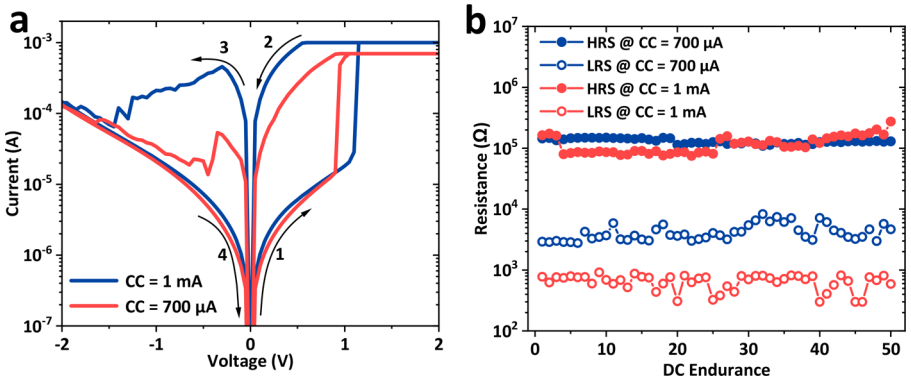


**Figure 7.** (a) $I-V$ characteristics of a Ag/PMMA/GeSbTe/TiN memristor (50% PMMA) for different CC. (b) DC endurance of the device showing the reproducible multistate resistance behavior under different CCs.

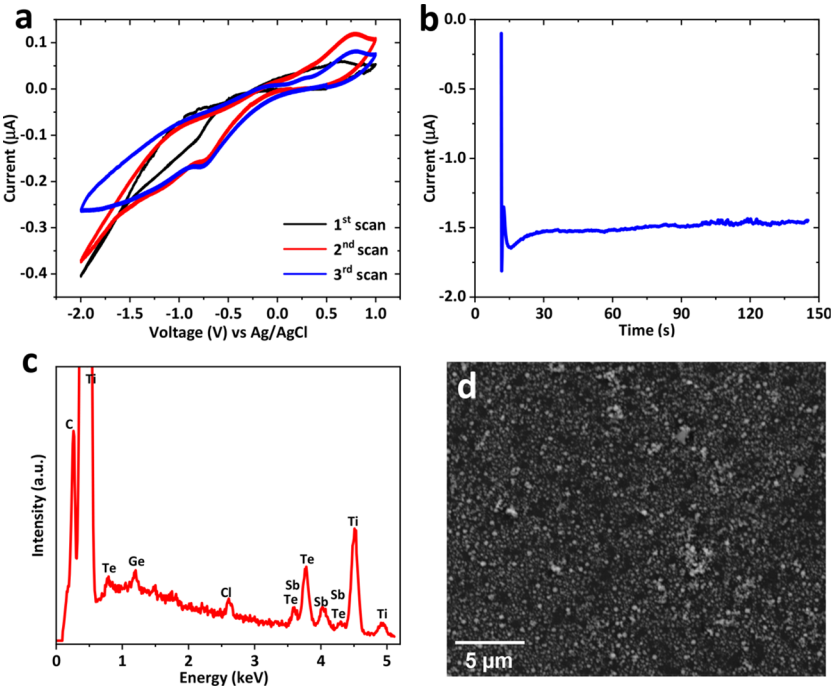


**Figure 8.** (a) CV of the 4-mm-diameter TiN/polyimide substrate in 0.1 M $[N^nBu_4]Cl$ electrolyte containing 2.5 mM $[N^nBu_4][GeCl_5]$, 1 mM $[N^nBu_4][SbCl_4]$, and 2 mM $[N^nBu_4]_2[TeCl_6]$. Scan rate: 50 mV $s^{-1}$. (b) Current time transient for GeSbTe electrodeposition on polyimide substrate at deposition potential of −1.75 V vs Ag/AgCl. The cutoff charge is −5 $\mu$C. (c) EDX spectrum of the electrodeposited GeSbTe on polyimide substrate showing the existence of Ge, Sb, and Te within the thin film. (d) SEM image of the GeSbTe thin film on TiN/polyimide substrate.

needed for both the SET and RESET processes to protect the devices.[41,56,71]

We will now demonstrate the development of hybrid PMMA/GeSbTe material-based memristor devices on flexible substrate. The GeSbTe thin film was electrodeposited on a polyimide substrate with a TiN layer as the bottom electrode. The cyclic voltammetry and deposition transient are shown in Figure 8a and b, respectively. The anodic stripping region of the cyclic voltammetry is similar to the deposition on Si supported TiN substrates in Figure 2; however, the peaks at the cathodic deposition region are less obvious on the flexible TiN substrates for the first scan. Subsequent CVs are similar to those shown in Figure 2a. The actual deposition is controlled by the same cutoff charge of −5 $\mu$C to achieve a nominal thickness of 100 nm. The GeSbTe composition of 7:20:73 was identified by EDX (shown in Figure 8c). The EDX spectrum also shows the presence of Cl, which is originated from the electrolyte. Top SEM image of the electrodeposited GeSbTe thin film is shown in Figure 8d. Furthermore, AFM image of the film is presented in Figure S4. The 33% PMMA concentration solution was selected to deposit the PMMA layer on the GeSbTe thin film to obtain the hybrid material structure.

A photographic image of the developed flexible hybrid memory devices with the structure of Ag/PMMA/GeSbTe/TiN under bending is shown in Figure 9a. In order to confirm the feasibility of our devices for flexible nonvolatile memory applications, mechanical flexibility test was carried out on a curved surface with a bending radius ($R$) of 15 mm. The effect of mechanical flexibility testing on the electronic properties of the flexible memristor device was investigated by performing $I-V$ sweeps before bending (black curve), during bending (blue curve), and after bending (red curve), as shown in Figure 9b. The device shows a bipolar resistive switching behavior


https://doi.org/10.1021/acsanm.2c03639
ACS Appl. Nano Mater. 2022, 5, 17711−17720

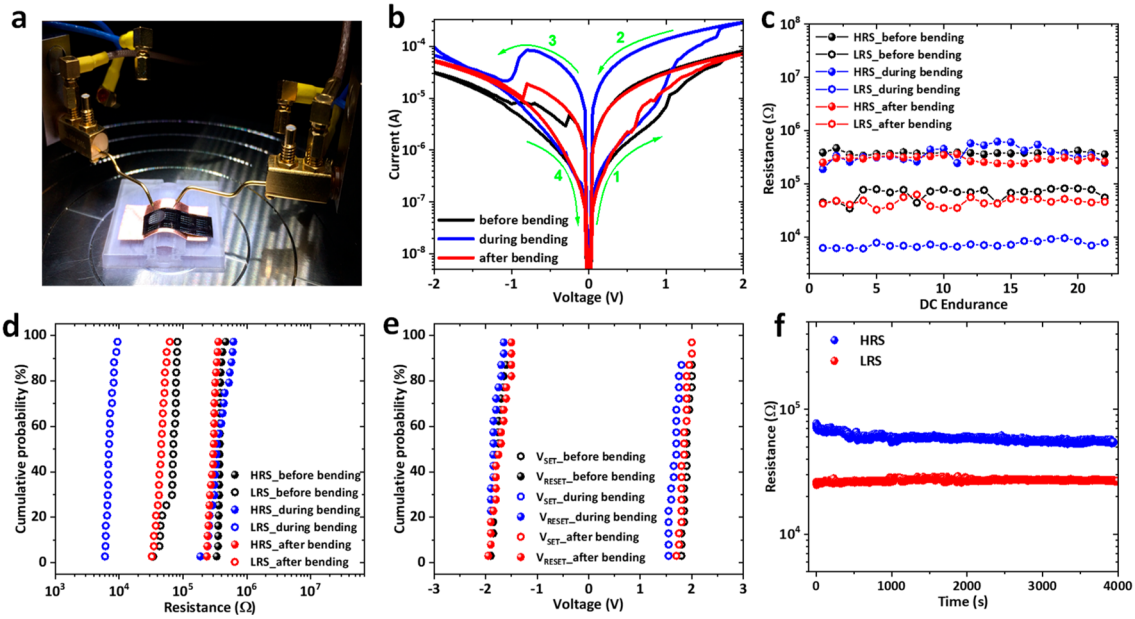


**Figure 9.** (a) A real photo image of a hybrid flexible memristor under bending radius ($R$) of 15 mm. (b) $I-V$ resistive switching characteristics of a flexible Ag/PMMA/GeSbTe/TiN device before bending (black curve), during bending (blue curve), and after bending (red curve). (c) Endurance characteristics of the device at a read voltage of 0.5 V. (d) Cumulative probability of HRS and LRS, and (e) $V_{SET}$ and $V_{RESET}$. (f) Retention test for the device after bending at a read voltage of 0.5 V.

with the SET and RESET processes occurred at positive and negative voltage polarities, respectively. The device exhibited reliable operation even under bending condition. It is interesting to note that the ON current is shifted to a higher level, increasing the ON/OFF ratio from 10 under flat condition to 33 under bending condition. The effect is reversible, and the ON current shifts back to its original starting position after bending. The higher ON current obtained here is likely to be induced by stretching the PMMA material upon bending, which could reduce the thickness of the PMMA and as a result reduces the resistance of the device.

To evaluate operational reliability of our hybrid flexible memristor, the memory performance properties including the DC endurance and cumulative probability for the ON/OFF resistance ratio were analyzed. As shown in Figure 9c, the device showed a stable endurance in the DC mode for both the HRS and LRS, and no degradation was observed under either flat or bending conditions. Figure 9d shows the high uniformity of cumulative probability distributions for the HRS and LRS under flat and bending conditions. Moreover, to examine the operational switching voltages uniformity of the device, cumulative probability distributions for the $V_{SET}$ and $V_{RESET}$ were also analyzed under flat and bending conditions as shown in Figure 9e. The plot shows excellent uniformity distribution for both switching voltages, which are desirable for nonvolatile RRAM applications. To further evaluate the reliability and stability of the device after bending conditions, retention performance was examined for the HRS and LRS at a continuous voltage of 0.5 V. Both HRS and LRS were found to be retained without degradation for over 4000 s, indicating the nonvolatility and good retention characteristics of the device as shown in Figure 9f. Further DC sweeps from another device also show a reproducible switching performance before, during, and after bending are reported in Supporting Information Figure S5. This suggests electrodeposition is a viable approach for fabricating flexible memristor devices.

## 3. CONCLUSIONS

In conclusion, we have successfully demonstrated the development of a flexible memristor that shows reliable bipolar resistive switching properties at low switching voltages. This is achieved by utilizing a hybrid organic–inorganic materials approach by incorporating PMMA with resistive switching electrodeposited GeSbTe nanoscale thin films. The switching mechanism in these devices is explained by the formation and rapture of conductive Ag filament(s) upon application of different electric field polarity. The resistance states can be controlled by CC, demonstrating the multistate switching behavior. Our approach for the fabrication of flexible memristor devices could have potential applications in future nonvolatile data storage electronics.

## 4. EXPERIMENTAL SECTION

The memristor devices consist of a vertical thin film stack with the following order of materials, Ag/PMMA/GeSbTe/TiN (Figure 3a). Prior to electrodeposition process of GeSbTe thin films, TiN bottom contacts (200 nm thick) were sputtered on silicon and polyamide substrates. The GeSbTe thin films were deposited on these substrates using the following procedure.

**Solution.** Electrolytes were prepared in anhydrous $CH_2Cl_2$ (Sigma-Aldrich, 95%), dried and degassed by refluxing with $CaH_2$, followed by distillation and then stored in the glovebox. A 0.1 M $[N^nBu_4]Cl$ (Sigma-Aldrich, ≥ 99.0%, dried) was used as the supporting electrolyte. The electrolyte contains 2.5 mM $[N^nBu_4][GeCl_5]$, 1 mM $[N^nBu_4][SbCl_4]$, and 2 mM $[N^nBu_4]_2[TeCl_6]$, which were synthesized as described previously.[61]

**Electrodes.** Silicon and polyamide substrates with predeposited TiN bottom electrodes serve as the electrode for electrodeposition. The detailed fabrication process can be found in our previous work.[47,72] A Pt/Ir (90%:10%) disk was employed as the counter electrode and an Ag/AgCl wire (0.1 M $[N^nBu_4]Cl$ in anhydrous $CH_2Cl_2$) was used as the reference electrode.


https://doi.org/10.1021/acsanm.2c03639
ACS Appl. Nano Mater. 2022, 5, 17711−17720

**Electrochemistry.** All cyclic voltammetry (CV) and electrodeposition experiments were carried out in a recirculating glovebox (Belle) to exclude moisture and air. Oxygen levels were kept below 10 ppm. A microAutolab 3 potentiostat and a Nova 1 software package were used for all electrochemical measurements. Prior to GeSbTe electrodeposition, voltammetry was recorded on a TiN bottom contact in $CH_2Cl_2$ solution containing 2.5 mM $[N^nBu_4]GeCl_5$, 1 mM $[N^nBu_4]SbCl_4$, and 2 mM $[N^nBu_4]_2TeCl_6$ at a scan rate of 50 mV $s^{-1}$, Figure 2a. On the first scan reduction starts at around −1 V, and there is evidence of a nucleation loop, consistent with deposition on the electrode surface, on the return scan. Similar behavior is seen on the second and third scans, although now the reduction current increases less steeply, possibly due to the presence of a semiconducting deposit of GeSbTe at the electrode surface. On the return scan a stripping peak is evident at +0.5 V. This voltammetry is broadly consistent with our earlier work.[47] Electrodeposition of GeSbTe was carried out at −1.75 V vs Ag/AgCl with a cutoff charge of 5 $\mu$C to allow a complete depositing GeSbTe thin film, as shown in Figure 2b. Electrodeposition was carried out by holding the TiN electrode at open circuit potential for the initial 5 s, followed by applying −1.75 V vs Ag/AgCl. The measurement stops automatically when the charge passed at the working electrode reaches 5 $\mu$C. The substrate was then rinsed in $CH_2Cl_2$ and stored in the glovebox.

**Device Fabrication and Characterization.** 495 poly(methyl methacrylate) (PMMA) solution, purchased from Sigma-Aldrich, was diluted in anisole in different ratios designed to give predefined PMMA concentration solutions, 20%, 25%, 33%, and 50%. The solutions were spin coated onto the pre-electrodeposited GeSbTe thin films at 4000 rpm for 60 s. The samples were then annealed at 120 °C for 3 min in air to remove any remaining solvent. Ag top electrodes (200 nm thick) were thermally deposited under vacuum conditions through a shadow mask containing 250-$\mu$m-diameter circles. Note that a control device consisting of GeSbTe (no PMMA) with a structure of Ag/GeSbTe/TiN was also fabricated. The electrical characteristics were measured at room temperature and ambient pressure using a probe connected to a Keysight (B1500) system. For all measurements, the voltage was applied to the top electrode Ag contacts, while the bottom electrode TiN contacts were grounded. SEM, EDX and AFM were used to characterize the thin films.

## ■ ASSOCIATED CONTENT

### Supporting Information

The Supporting Information is available free of charge at https://pubs.acs.org/doi/10.1021/acsanm.2c03639.

Extra details of thickness characterization, electrical characterization, and AFM image (PDF)

## ■ AUTHOR INFORMATION


### Corresponding Authors

**Ayoub H. Jaafar** − *School of Electronics and Computer Science, University of Southampton, Southampton SO17 1BJ, United Kingdom; School of Physics and Astronomy, University of Nottingham, Nottingham NG7 2RD, United Kingdom;* orcid.org/0000-0001-7305-4542; Email: a.h.j.hamdiyah@soton.ac.uk

**Philip N. Bartlett** − *School of Chemistry, University of Southampton, Southampton SO17 1BJ, United Kingdom;* Email: p.n.bartlett@soton.ac.uk

**Ruomeng Huang** − *School of Electronics and Computer Science, University of Southampton, Southampton SO17 1BJ, United Kingdom;* orcid.org/0000-0003-1185-635X; Email: r.huang@soton.ac.uk

### Authors

**Lingcong Meng** − *School of Chemistry, University of Southampton, Southampton SO17 1BJ, United Kingdom; School of Chemistry, University of Lincoln, Lincoln LN6 7TS, United Kingdom*

**Tongjun Zhang** − *School of Electronics and Computer Science, University of Southampton, Southampton SO17 1BJ, United Kingdom*

**Dongkai Guo** − *School of Electronics and Computer Science, University of Southampton, Southampton SO17 1BJ, United Kingdom*

**Daniel Newbrook** − *School of Electronics and Computer Science, University of Southampton, Southampton SO17 1BJ, United Kingdom*

**Wenjian Zhang** − *School of Chemistry, University of Southampton, Southampton SO17 1BJ, United Kingdom*

**Gillian Reid** − *School of Chemistry, University of Southampton, Southampton SO17 1BJ, United Kingdom;* orcid.org/0000-0001-5349-3468

**C. H. de Groot** − *School of Electronics and Computer Science, University of Southampton, Southampton SO17 1BJ, United Kingdom;* orcid.org/0000-0002-3850-7101

Complete contact information is available at: https://pubs.acs.org/10.1021/acsanm.2c03639


### Author Contributions

The manuscript was written through contributions of all authors. All authors have given approval to the final version of the manuscript.

### Notes

The authors declare no competing financial interest.

Data supporting this study are openly available from the University of Southampton repository at DOI: https://doi.org/10.5258/SOTON/D2440. Additional data from this study are available from the corresponding author upon reasonable request.

## ■ ACKNOWLEDGMENTS

This work is part of the ADEPT project funded by a Programme Grant from the EPSRC (EP/N035437/1).

## ■ REFERENCES


(1) Sharma, B. K.; Ahn, J. H. Flexible and Stretchable Oxide Electronics. *Adv. Electron. Mater.* **2016**, *2*, 1600105.

(2) Biggs, J.; Myers, J.; Kufel, J.; Ozer, E.; Craske, S.; Sou, A.; Ramsdale, C.; Williamson, K.; Price, R.; White, S. A Natively Flexible 32-Bit Arm Microprocessor. *Nature* **2021**, *595*, 532−536.

(3) Nomura, K.; Ohta, H.; Takagi, A.; Kamiya, T.; Hirano, M.; Hosono, H. Room-Temperature Fabrication of Transparent Flexible Thin-Film Transistors Using Amorphous Oxide Semiconductors. *Nature* **2004**, *432*, 488−492.

(4) Gelinck, G. H.; Huitema, H. E. A.; van Veenendaal, E.; Cantatore, E.; Schrijnemakers, L.; van der Putten, J. B. P. H.; Geuns, T. C. T.; Beenhakkers, M.; Giesbers, J. B.; Huisman, B.-H.; Meijer, E. J.; Benito, E. M.; Touwslager, F. J.; Marsman, A. W.; van Rens, B. J. E.; de Leeuw, D. M. Flexible Active-Matrix Displays and Shift Registers Based on Solution-Processed Organic Transistors. *Nat. Mater.* **2004**, *3*, 106−110.

(5) Han, S. T.; Zhou, Y.; Roy, V. A. L. Towards the Development of Flexible Non-Volatile Memories. *Adv. Mater.* **2013**, *25*, 5425−5449.

(6) Wang, J.; Wang, F.; Yin, L.; Sendeku, M. G.; Zhang, Y.; Cheng, R.; Wang, Z.; Li, N.; Huang, W.; He, J. A Unipolar Nonvolatile Resistive Switching Behavior in a Layered Transition Metal Oxide. *Nanoscale* **2019**, *11*, 20497−20506.

(7) Choi, B. J.; Torrezan, A. C.; Strachan, J. P.; Kotula, P. G.; Lohn, A. J.; Marinella, M. J.; Li, Z.; Williams, R. S.; Yang, J. J. High-Speed

and Low-Energy Nitride Memristors. *Adv. Funct. Mater.* **2016**, *26*, 5290−5296.
(8) Li, C.; Belkin, D.; Li, Y.; Yan, P.; Hu, M.; Ge, N.; Jiang, H.; Montgomery, E.; Lin, P.; Wang, Z.; Song, W.; Strachan, J. P.; Barnell, M.; Wu, Q.; Williams, R. S.; Yang, J. J.; Xia, Q. Efficient and Self-Adaptive in-Situ Learning in Multilayer Memristor Neural Networks. *Nat. Commun.* **2018**, *9*, 1−8.
(9) Jaafar, A. H.; Kemp, N. T. Wavelength Dependent Light Tunable Resistive Switching Graphene Oxide Nonvolatile Memory Devices. *Carbon N Y* **2019**, *153*, 81−88.
(10) Jaafar, A. H.; Gee, A.; Kemp, N. T. Nanorods Versus Nanoparticles: A Comparison Study of Au/ZnO-PMMA/Au Non-Volatile Memory Devices Showing the Importance of Nanostructure Geometry on Conduction Mechanisms and Switching Properties. *IEEE Trans. Nanotechnol.* **2020**, *19*, 236−246.
(11) Jaafar, A. H.; O'Neill, M.; Kelly, S. M.; Verrelli, E.; Kemp, N. T. Percolation Threshold Enables Optical Resistive-Memory Switching and Light-Tuneable Synaptic Learning in Segregated Nanocomposites. *Adv. Electron. Mater.* **2019**, *5*, 1900197.
(12) Jaafar, A. H.; Gray, R. J.; Verrelli, E.; O'Neill, M.; Kelly, S. M.; Kemp, N. T. Reversible Optical Switching Memristors with Tunable STDP Synaptic Plasticity: A Route to Hierarchical Control in Artificial Intelligent Systems. *Nanoscale* **2017**, *9*, 17091−17098.
(13) Jaafar, A. H.; al Chawa, M. M.; Cheng, F.; Kelly, S. M.; Picos, R.; Tetzlaff, R.; Kemp, N. T. Polymer/TiO 2 Nanorod Nanocomposite Optical Memristor Device. *J. Phys. Chem. C* **2021**, *125*, 14965−14973.
(14) Carlos, E.; Branquinho, R.; Martins, R.; Kiazadeh, A.; Fortunato, E. Recent Progress in Solution-Based Metal Oxide Resistive Switching Devices. *Adv. Mater.* **2021**, *33*, 2004328.
(15) Goswami, S.; Matula, A. J.; Rath, S. P.; Hedström, S.; Saha, S.; Annamalai, M.; Sengupta, D.; Patra, A.; Ghosh, S.; Jani, H.; Sarkar, S.; Motapothula, M. R.; Nijhuis, C. A.; Martin, J.; Goswami, S.; Batista, V. S.; Venkatesan, T. Robust Resistive Memory Devices Using Solution-Processable Metal-Coordinated Azo Aromatics. *Nat. Mater.* **2017**, *16*, 1216−1224.
(16) Nau, S.; Wolf, C.; Sax, S.; List-Kratochvil, E. J. W. Organic Non-Volatile Resistive Photo-Switches for Flexible Image Detector Arrays. *Adv. Mater.* **2015**, *27*, 1048−1052.
(17) Ge, R.; Wu, X.; Kim, M.; Shi, J.; Sonde, S.; Tao, L.; Zhang, Y.; Lee, J. C.; Akinwande, D. Atomristor: Nonvolatile Resistance Switching in Atomic Sheets of Transition Metal Dichalcogenides. *Nano Lett.* **2018**, *18*, 434−441.
(18) Feng, X.; Li, Y.; Wang, L.; Chen, S.; Yu, Z. G.; Tan, W. C.; Macadam, N.; Hu, G.; Huang, L.; Chen, L.; Gong, X.; Chi, D.; Hasan, T.; Thean, A. V. Y.; Zhang, Y. W.; Ang, K. W. A Fully Printed Flexible MoS2Memristive Artificial Synapse with Femtojoule Switching Energy. *Adv. Electron. Mater.* **2019**, *5*, 1970061.
(19) Zou, L. Multilevel Resistive Switching Performance of TiO2-Based Flexible Memory Prepared by Low-Temperature Sol-Gel Method with UV Irradiation. *Curr. Appl. Phys.* **2021**, *24*, 32−38.
(20) Kim, S.; Son, J. H.; Lee, S. H.; You, B. K.; Park, K. il; Lee, H. K.; Byun, M.; Lee, K. J. Flexible Crossbar-Structured Resistive Memory Arrays on Plastic Substrates via Inorganic-Based Laser Lift-Off. *Adv. Mater.* **2014**, *26*, 7480−7487.
(21) Kim, S.; Jeong, H. Y.; Kim, S. K.; Choi, S. Y.; Lee, K. J. Flexible Memristive Memory Array on Plastic Substrates. *Nano Lett.* **2011**, *11*, 5438−5442.
(22) Jeong, H. Y.; Kim, J. Y.; Kim, J. W.; Hwang, J. O.; Kim, J. E.; Lee, J. Y.; Yoon, T. H.; Cho, B. J.; Kim, S. O.; Ruoff, R. S.; Choi, S. Y. Graphene Oxide Thin Films for Flexible Nonvolatile Memory Applications. *Nano Lett.* **2010**, *10*, 4381−4386.
(23) Das, U.; Nyayban, A.; Paul, B.; Barman, A.; Sarkar, P.; Roy, A. Compliance Current-Dependent Dual-Functional Bipolar and Threshold Resistive Switching in All-Inorganic Rubidium Lead-Bromide Perovskite-Based Flexible Device. *ACS Appl. Electron. Mater.* **2020**, *2*, 1343−1351.
(24) Xu, M.; Mai, X.; Lin, J.; Zhang, W.; Li, Y.; He, Y.; Tong, H.; Hou, X.; Zhou, P.; Miao, X. Recent Advances on Neuromorphic Devices Based on Chalcogenide Phase-Change Materials. *Adv. Funct. Mater.* **2020**, *30*, 2003419.
(25) Wuttig, M.; Yamada, N. Phase-Change Materials for Rewriteable Data Storage. *Nat. Mater.* **2007**, *6*, 824−832.
(26) Cheng, H. Y.; Raoux, S.; Chen, Y. C. The Impact of Film Thickness and Melt-Quenched Phase on the Phase Transition Characteristics of Ge2 Sb2 Te5. *J. Appl. Phys.* **2010**, *107*, 074308.
(27) Pandian, R.; Kooi, B. J.; Palasantzas, G.; de Hosson, J. T. M.; Pauza, A. Nanoscale Electrolytic Switching in Phase-Change Chalcogenide Films. *Adv. Mater.* **2007**, *19*, 4431−4437.
(28) Deleruyelle, D.; Putero, M.; Ouled-Khachroum, T.; Bocquet, M.; Coulet, M. v.; Boddaert, X.; Calmes, C.; Muller, C. Ge2Sb2Te5 Layer Used as Solid Electrolyte in Conductive-Bridge Memory Devices Fabricated on Flexible Substrate. *Solid-State Electron.* **2013**, *79*, 159−165.
(29) Huang, Y. H.; Chen, H. A.; Wu, H. H.; Hsieh, T. E. Forming-Free, Bi-Directional Polarity Conductive-Bridge Memory Devices with Ge2Sb2Te5 Solid-State Electrolyte and Ag Active Electrode. *J. Appl. Phys.* **2015**, *117*, 014505.
(30) Lee, W.; Siddik, M.; Jung, S.; Park, J.; Kim, S.; Shin, J.; Lee, J.; Park, S.; Son, M.; Hwang, H. Effect of Ge2Sb2Te5 Thermal Barrier on Reset Operations in Filament-Type Resistive Memory. *IEEE Electron Device Lett.* **2011**, *32*, 1573−1575.
(31) Lv, H.; Wan, H.; Tang, T. Improvement of Resistive Switching Uniformity by Introducing a Thin GST Interface Layer. *IEEE Electron Device Lett.* **2010**, *31*, 978−980.
(32) Rebora, C.; Huang, R.; Kissling, G. P.; Bocquet, M.; Groot, K. de; Favre, L.; Grosso, D.; Deleruyelle, D.; Putero, M. Conductive-Bridge Memory Cells Based on a Nanoporous Electrodeposited GeSbTe Alloy. *Nanotechnology* **2019**, *30*, 025202.
(33) Zhang, Z.; Wang, Y.; Wang, G.; Mu, J.; Ma, M.; He, Y.; Yang, R.; Li, H. Electrochemical Metallization Cell with Solid Phase Tunable Ge2Sb2Te5 Electrolyte. *Sci. Rep.* **2018**, *8*, 1−7.
(34) Kozicki, M. N.; Park, M.; Mitkova, M. Nanoscale Memory Elements Based on Solid-State Electrolytes. *IEEE Trans. Nanotechnol.* **2005**, *4*, 331−338.
(35) Kim, C.-J.; Yoon, S.-G.; Choi, K.-J.; Ryu, S.-O.; Yoon, S.-M.; Lee, N.-Y.; Yu, B.-G. Characterization of Silver-Saturated Ge−Te Chalcogenide Thin Films for Nonvolatile Random Access Memory. *J. Vac. Sci. Technol. B* **2006**, *24*, 721−724.
(36) Li, Y.; Zhong, Y.; Xu, L.; Zhang, J.; Xu, X.; Sun, H.; Miao, X. Ultrafast Synaptic Events in a Chalcogenide Memristor. *Sci. Rep.* **2013**, *3*, 1−7.
(37) Pandian, R.; Kooi, B. J.; Palasantzas, G.; de Hosson, J. T. M.; Pauza, A. Polarity-Dependent Reversible Resistance Switching in Ge-Sb-Te Phase-Change Thin Films. *Appl. Phys. Lett.* **2007**, *91*, 152103.
(38) Pandian, R.; Kooi, B. J.; Oosthoek, J. L. M.; van den Dool, P.; Palasantzas, G.; Pauza, A. Polarity-Dependent Resistance Switching in GeSbTe Phase-Change Thin Films: The Importance of Excess Sb in Filament Formation. *Appl. Phys. Lett.* **2009**, *95*, 252109.
(39) Woo, J.; Jung, S.; Siddik, M.; Cha, E.; Md. Sadaf, S.; Hwang, H. Effect of Interfacial Oxide Layer on the Switching Uniformity of Ge 2Sb2Te5-Based Resistive Change Memory Devices. *Appl. Phys. Lett.* **2011**, *99*, 162109.
(40) Yoo, S.; Eom, T.; Gwon, T.; Hwang, C. S. Bipolar Resistive Switching Behavior of an Amorphous Ge2Sb2Te5 Thin Films with a Te Layer. *Nanoscale* **2015**, *7*, 6340−6347.
(41) Jaafar, A. H.; Meng, L.; Noori, Y. J.; Zhang, W.; Han, Y.; Beanland, R.; Smith, D. C.; Reid, G.; de Groot, K.; Huang, R.; Bartlett, P. N. Electrodeposition of GeSbTe-Based Resistive Switching Memory in Crossbar Arrays. *J. Phys. Chem. C* **2021**, *125*, 26247−26255.
(42) Raoux, S.; Welnic, W.; Ielmini, D. Phase Change Materials and Their Application to Nonvolatile Memories. *Chem. Rev.* **2010**, *110*, 240−267.
(43) Andricacos, P. C. Copper On-Chip Interconnections: A Breakthrough in Electrodeposition to Make Better Chips To Make Better Chips. *Electrochem. Soc. Interface* **1999**, *8*, 32−37.


https://doi.org/10.1021/acsanm.2c03639
*ACS Appl. Nano Mater.* 2022, 5, 17711−17720

(44) Andricacos, P. C.; Uzoh, C.; Dukovic, J. O.; Horkans, J.; Deligianni, H. Damascene Copper for Chip Interconnections. *IBM J. Res. Dev.* **1998**, *42*, 567−574.
(45) Huang, R.; Kissling, G. P.; Jolleys, A.; Bartlett, P. N.; Hector, A. L.; Levason, W.; Reid, G.; de Groot, C. H. 'Kees.' Phase-Change Memory Properties of Electrodeposited Ge-Sb-Te Thin Film. *Nanoscale Res. Lett.* **2015**, *10*, 1−7.
(46) Bartlett, P. N.; Benjamin, S. L.; Kees De Groot, C. H.; Hector, A. L.; Huang, R.; Jolleys, A.; Kissling, G. P.; Levason, W.; Pearce, S. J.; Reid, G.; Wang, Y. Non-Aqueous Electrodeposition of Functional Semiconducting Metal Chalcogenides: Ge2Sb2Te5 Phase Change Memory. *Mater. Horiz.* **2015**, *2*, 420−426.
(47) Huang, R.; Kissling, G. P.; Kashtiban, R.; Noori, Y. J.; Cicvarić, K.; Zhang, W.; Hector, A. L.; Beanland, R.; Smith, D. C.; Reid, G.; Bartlett, P. N.; de Groot, C. H. (Kees). Towards a 3D GeSbTe Phase Change Memory with Integrated Selector by Non-Aqueous Electrodeposition. *Faraday Discuss.* **2019**, *213*, 339−355.
(48) Wu, L.; Guo, J.; Zhong, W.; Zhang, W.; Kang, X.; Chen, W.; Du, Y. Flexible, Multilevel, and Low-Operating-Voltage Resistive Memory Based on MoS2 − RGO Hybrid. *Appl. Surf. Sci.* **2019**, *463*, 947−952.
(49) An, H.; Lee, Y. H.; Lee, J. H.; Wu, C.; Koo, B. M.; Kim, T. W. Highly Stable and Flexible Memristive Devices Based on Polyvinylpyrrolidone: WS2 Quantum Dots. *Sci. Rep.* **2020**, *10*, 1−8.
(50) Nagareddy, V. K.; Barnes, M. D.; Zipoli, F.; Lai, K. T.; Alexeev, A. M.; Craciun, M. F.; Wright, C. D. Multilevel Ultrafast Flexible Nanoscale Nonvolatile Hybrid Graphene Oxide-Titanium Oxide Memories. *ACS Nano* **2017**, *11*, 3010−3021.
(51) Son, D. I.; Kim, T. W.; Shim, J. H.; Jung, J. H.; Lee, D. U.; Lee, J. M.; Park, W. il; Choi, W. K. Flexible Organic Bistable Devices Based on Graphene Embedded in an Insulating Poly(Methyl Methacrylate) Polymer Layer. *Nano Lett.* **2010**, *10*, 2441−2447.
(52) Son, D.-I.; Kim, J.-H.; Park, D.-H.; Choi, W. K.; Li, F.; Ham, J. H.; Kim, T. W. Nonvolatile Flexible Organic Bistable Devices Fabricated Utilizing CdSe/ZnS Nanoparticles Embedded in a Conducting Poly N-Vinylcarbazole Polymer Layer. *Nanotechnology* **2008**, *19*, 055204.
(53) Son, D.; Park, D.; Choi, W. K.; Cho, S.; Kim, W.; Kim, T. W. Carrier Transport in Flexible Organic Bistable Devices of ZnO Nanoparticles Embedded in an Insulating Poly (Methyl Methacrylate) Polymer Layer. *Nanotechnology* **2009**, *20*, 195203.
(54) Gu, C.; Lee, J. S. Flexible Hybrid Organic-Inorganic Perovskite Memory. *ACS Nano* **2016**, *10*, 5413−5418.
(55) Ribierre, J. C.; Aoyama, T.; Muto, T.; André, P. Hybrid Organic-Inorganic Liquid Bistable Memory Devices. *Org. Electron.* **2011**, *12*, 1800−1805.
(56) Hwang, B.; Lee, J. S. Lead-Free, Air-Stable Hybrid Organic-Inorganic Perovskite Resistive Switching Memory with Ultrafast Switching and Multilevel Data Storage. *Nanoscale* **2018**, *10*, 8578−8584.
(57) Choi, J.; Park, S.; Lee, J.; Hong, K.; Kim, D. H.; Moon, C. W.; Park, G. do; Suh, J.; Hwang, J.; Kim, S. Y.; Jung, H. S.; Park, N. G.; Han, S.; Nam, K. T.; Jang, H. W. Organolead Halide Perovskites for Low Operating Voltage Multilevel Resistive Switching. *Adv. Mater.* **2016**, *28*, 6562−6567.
(58) Seo, J. Y.; Choi, J.; Kim, H. S.; Kim, J.; Yang, J. M.; Cuhadar, C.; Han, J. S.; Kim, S. J.; Lee, D.; Jang, H. W.; Park, N. G. Wafer-Scale Reliable Switching Memory Based on 2-Dimensional Layered Organic-Inorganic Halide Perovskite. *Nanoscale* **2017**, *9*, 15278−15285.
(59) Han, J. S.; Le, Q. V.; Choi, J.; Hong, K.; Moon, C. W.; Kim, T. L.; Kim, H.; Kim, S. Y.; Jang, H. W. Air-Stable Cesium Lead Iodide Perovskite for Ultra-Low Operating Voltage Resistive Switching. *Adv. Funct. Mater.* **2018**, *28*, 1705783.
(60) Bartlett, P. N.; Cook, D.; de Groot, C. H.; Hector, A. L.; Huang, R.; Jolleys, A.; Kissling, G. P.; Levason, W.; Pearce, S. J.; Reid, G. Non-Aqueous Electrodeposition of p-Block Metals and Metalloids from Halometallate Salts. *RSC Adv.* **2013**, *3*, 15645−15654.
(61) Kissling, G. P.; Huang, R.; Jolleys, A.; Benjamin, S. L.; Hector, A. L.; Reid, G.; Levason, W.; de Groot, C. H.; Bartlett, P. N. Electrodeposition of a Functional Solid State Memory Material: Germanium Antimony Telluride from a Non-Aqueous Plating Bath. *J. Electrochem. Soc.* **2018**, *165*, D557−D567.
(62) Qi, J.; Olmedo, M.; Ren, J.; Zhan, N.; Zhao, J.; Zheng, J. G.; Liu, J. Resistive Switching in Single Epitaxial ZnO Nanoislands. *ACS Nano* **2012**, *6*, 1051−1058.
(63) Sun, Y.; Yan, X.; Zheng, X.; Liu, Y.; Zhao, Y.; Shen, Y.; Liao, Q.; Zhang, Y. High On-off Ratio Improvement of ZnO-Based Forming-Free Memristor by Surface Hydrogen Annealing. *ACS Appl. Mater. Interfaces* **2015**, *7*, 7382−7388.
(64) Nau, S.; Sax, S.; List-Kratochvil, E. J. W. Unravelling the Nature of Unipolar Resistance Switching in Organic Devices by Utilizing the Photovoltaic Effect. *Adv. Mater.* **2014**, *26*, 2508−2513.
(65) Yang, Y.; Gao, P.; Li, L.; Pan, X.; Tappertzhofen, S.; Choi, S.; Waser, R.; Valov, I.; Lu, W. D. Electrochemical Dynamics of Nanoscale Metallic Inclusions in Dielectrics. *Nat. Commun.* **2014**, *5*, 1−9.
(66) Verrelli, E.; Gray, R. J.; O'Neill, M.; Kelly, S. M.; Kemp, N. T. Microwave Oven Fabricated Hybrid Memristor Devices for Non-Volatile Memory Storage. *Mater. Res. Express.* **2014**, *1*, 046305.
(67) Petzold, S.; Piros, E.; Eilhardt, R.; Zintler, A.; Vogel, T.; Kaiser, N.; Radetinac, A.; Komissinskiy, P.; Jalaguier, E.; Nolot, E.; Charpin-Nicolle, C.; Wenger, C.; Molina-Luna, L.; Miranda, E.; Alff, L. Tailoring the Switching Dynamics in Yttrium Oxide-Based RRAM Devices by Oxygen Engineering: From Digital to Multi-Level Quantization toward Analog Switching. *Adv. Electron. Mater.* **2020**, *6*, 2070044.
(68) He, C.; Shi, Z.; Zhang, L.; Yang, W.; Yang, R.; Shi, D.; Zhang, G. Multilevel Resistive Switching in Planar Graphene/SiO 2 Nanogap Structures. *ACS Nano* **2012**, *6*, 4214−4221.
(69) Shen, Z.; Zhao, C.; Kang, L.; Sun, Y.; Liu, Y.; Mitrovic, I. Z.; Yang, L.; Lim, E. G.; Zeng, Z.; Zhao, C. Emerging Optical In-Memory Computing Sensor Synapses Based on Low-Dimensional Nanomaterials for Neuromorphic Networks. *Adv. Intell. Syst.* **2022**, *4*, 2100236.
(70) Wang, Y.; Lv, Z.; Liao, Q.; Shan, H.; Chen, J.; Zhou, Y.; Zhou, L.; Chen, X.; Roy, V. A. L.; Wang, Z.; Xu, Z.; Zeng, Y. J.; Han, S. T. Synergies of Electrochemical Metallization and Valance Change in All-Inorganic Perovskite Quantum Dots for Resistive Switching. *Adv. Mater.* **2018**, *30*, 1870207.
(71) Zhao, X.; Fan, Z.; Xu, H.; Wang, Z.; Xu, J.; Ma, J.; Liu, Y. Reversible Alternation between Bipolar and Unipolar Resistive Switching in Ag/MoS2/Au Structure for Multilevel Flexible Memory. *J. Mater. Chem. C Mater.* **2018**, *6*, 7195−7200.
(72) Noori, Y. J.; Meng, L.; Jaafar, A. H.; Zhang, W.; Kissling, G. P.; Han, Y.; Abdelazim, N.; Zhelev, N.; Huang, R.; Beanland, R.; Smith, D. C.; Reid, G.; Groot, K. de; Bartlett, P. N. Phase Change Memory by GeSbTe Electrodeposition in Crossbar Arrays. *ACS Appl. Electron. Mater.* **2021**, *3*, 3610−3618.


https://doi.org/10.1021/acsanm.2c03639
*ACS Appl. Nano Mater.* 2022, 5, 17711−17720